

## **Fabricating Functionally Graded Materials by Ceramic On-Demand Extrusion with Dynamic Mixing**

Wenbin Li<sup>1</sup>, Austin J. Martin<sup>2</sup>, Benjamin Kroehler<sup>1</sup>, Alexander Henderson<sup>1</sup>, Tieshu Huang<sup>3</sup>, Jeremy Watts<sup>2</sup>, Gregory E. Hilmas<sup>2</sup> and Ming C. Leu<sup>1</sup>

<sup>1</sup>Department of Mechanical and Aerospace Engineering, Missouri University of Science and Technology, Rolla, Missouri, USA

<sup>2</sup>Department of Materials Science and Engineering, Missouri University of Science and Technology, Rolla, Missouri, USA

<sup>3</sup>NNSA's Kansas City National Security Campus, Kansas City, MO 64147, USA

### **Abstract**

Ceramic On-Demand Extrusion (CODE) is an extrusion-based additive manufacturing process recently developed for fabricating dense, functional ceramic components. Presented in this paper is a further development of this process focusing on fabrication of functionally graded materials (FGM). A dynamic mixing mechanism was developed for mixing constituent ceramic pastes, and an extrusion control scheme was developed for fabricating specimens with desired material compositions graded in real time. FGM specimens with compositions graded between Al<sub>2</sub>O<sub>3</sub> and ZrO<sub>2</sub> were fabricated and ultimately densified by sintering to validate the effectiveness of the CODE process for FGM fabrication. Energy dispersive spectroscopy (EDS) was used to compare final compositions to the original material designs. The specimen's hardness at different locations along the gradients was examined by micro-indentation tests. The dimensions of sintered specimens were measured, and the effects of material composition gradients on the distortions of sintered FGM specimens were analyzed.

### **Introduction**

Several additive manufacturing (AM) processes have been developed for ceramics and glasses, including binder jetting [1], [2], material extrusion [3]–[8], vat photopolymerization [9], [10], powder bed fusion [11, 12], and directed energy deposition [13–15], among others. Ceramic On-Demand Extrusion (CODE) [7] is a recently developed paste extrusion-based AM process, which produces ceramic components with near theoretical density (>98%) after sintering [4, 16–18]. It deposits high solids loading (>50 vol%) aqueous ceramic pastes onto a substrate layer by layer at room temperature. Each deposited layer is partially solidified by uniform infrared radiation drying from above before the subsequent layer is initiated. At the same time, undesirable evaporation from the sides of the part is prohibited by surrounding the part with a liquid [7]. This layered uniform radiation drying approach minimizes the moisture content gradient in the part

during the fabrication process and thus enables CODE to produce crack-free ceramic parts. The printed parts are then bulk-dried in a controlled environment with appropriate humidity, after which the green bodies are sintered to produce near-theoretical density parts [16–18].

Functionally graded materials (FGM) are characterized by gradual variations of material compositions over volumes, which allows for a combination of materials or material properties not typically achievable in monolithic materials [19]–[22]. Alumina/zirconia ( $\text{Al}_2\text{O}_3/\text{ZrO}_2$ ) FGM components have been of great interest, mainly to enhance the fracture toughness through the incorporation of  $\text{ZrO}_2$  phase. One potential application is the prosthetic hip joint ball [22, 23], where the FGM realizes the transition from a tough  $\text{ZrO}_2$  core, which provides the high strength of the hub structure and reduces the risk of cracking, to a wear-resistant  $\text{Al}_2\text{O}_3$  ball surface, which guarantees a long service life in a human body. Additive manufacturing (AM) processes are especially advantageous for fabricating FGM components due to the layer-by-layer nature of the processes. Considering that the melting temperatures of ceramics are usually too high for thermal-based melt deposition and the fact that the ink jetting-based ceramic AM processes are subject to high porosity [20], material extrusion-based AM processes are the most favorable method for fabricating ceramic FGM components [20].

The present paper introduces a dynamic mixing device to the Ceramic On-Demand Extrusion (CODE) system for fabricating FGM specimens. Two distinct materials were extruded through separate extruders into the mixing chamber of the dynamic mixer with controlled flowrates. The pastes were then blended by the dynamic mixer to a homogenous mixture and finally deposited through nozzles to fabricate FGM specimens with planned material compositional distribution. The FGM specimens were post-processed and characterized to validate the functionality and accuracy of the dynamic mixing device. Deformation was observed on the sintered specimens. The effects of material composition gradients on the deformation of sintered FGM specimens were analyzed.

### **Experimental Setup**

The CODE fabrication system consists of a cartesian gantry system, an extrusion device mounted on the gantry and capable of extruding viscous ceramic pastes at controlled flowrates, an oil feeding device to regulate the oil level in the tank, and an infrared radiation heating device capable of positioning the infrared source and providing on/off control. Introduction and details of the CODE fabrication system were presented in the previous papers [4, 7, 24]. In the present work, the CODE system was configured to deposit a mixture of two materials using a dynamic mixing tool head consisting of two auger extruders and a dynamic mixer. The two auger extruders were controlled separately to extrude two different pastes at independent flowrates. As shown in Figure 1(a), the two pastes are extruded through the inlets into the dynamic mixer. As the two pastes passed through the mixing chamber, a motor-driven mixing blade blended the distinct pastes to produce a homogenous mixture, which was then deposited through the outlet to form a 3D part. The actual components and layout of the dynamic mixing tool head are shown in Figure 1(b).

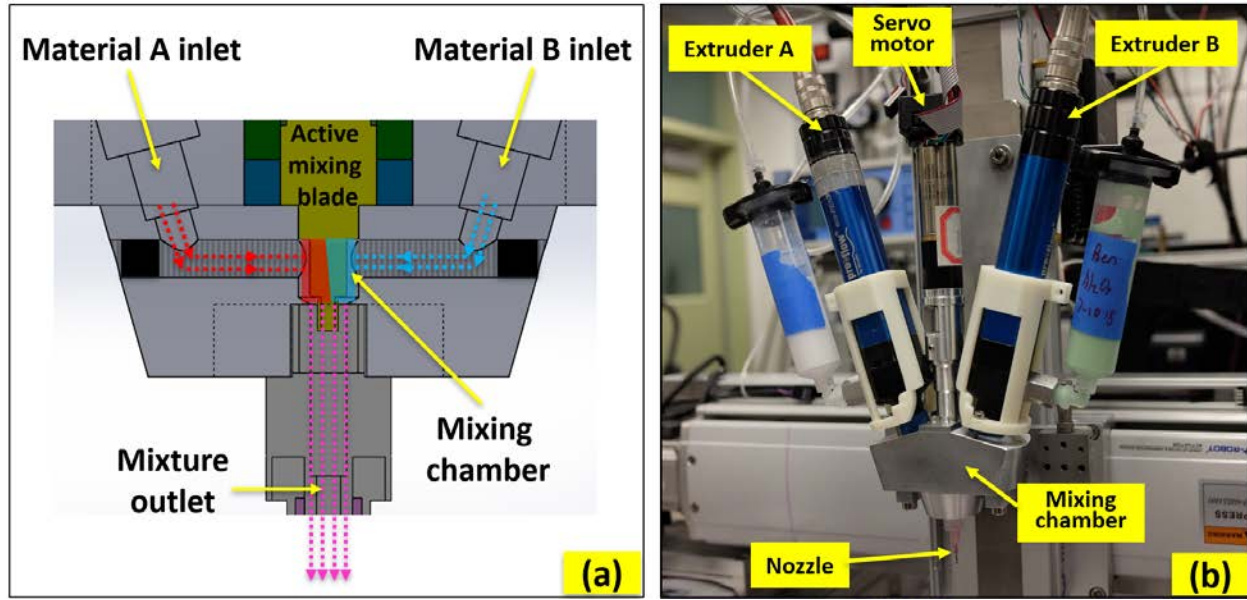


Figure 1. Dynamic mixing tool head of the CODE system. (a) Schematic of the dynamic mixer, (b) The actual dynamic mixing tool head mounted on the CODE system.

## Fabrication of Functionally Graded Materials

### Preparation of pastes

Aqueous  $\text{Al}_2\text{O}_3$  pastes and  $\text{ZrO}_2$  (3Y) pastes were prepared as the feedstock materials. The composition of the pastes and detailed steps of paste formation can be found in previous works [16, 17]. The  $\text{ZrO}_2$  pastes were prepared to have 50 vol% solids loading. Considering the shrinkage of components during the bulk drying process and the sintering process, the  $\text{Al}_2\text{O}_3$  pastes were also adjusted to have 50 vol% solids loading, expecting to minimize the mismatch of shrinkage between the two materials, and hence minimize the distortion of the FGM specimens during sintering. In order to visualize the material variation in the printed specimens, the white  $\text{Al}_2\text{O}_3$  pastes and  $\text{ZrO}_2$  pastes were colored green and pink, respectively, using FD&C Yellow 5 & Blue 1 and FD&C Red 40 dyes.

### Printing single-bead lines with graded materials

In order to test the capability of the dynamic mixing tool head to build parts with graded materials and examine the response of changing material composition, a single-bead serpentine shape was printed using both the  $\text{ZrO}_2$  paste (pink) and the  $\text{Al}_2\text{O}_3$  paste (green). The  $\text{ZrO}_2$  and  $\text{Al}_2\text{O}_3$  pastes were extruded by extruders A and B, respectively. As shown in Figure 2, the dynamic mixing tool head was first loaded with  $\text{ZrO}_2$  paste and was then commanded to switch to  $\text{Al}_2\text{O}_3$  paste by turning off extruder A and turning on the extruder B at location 1. The serpentine shape was printed from location 1 to location 5, during which the dynamic mixing tool head was commanded to switch between  $\text{ZrO}_2$  and  $\text{Al}_2\text{O}_3$  at locations 2, 3, and 4. The mixing blade was spinning at 900 rpm during the entire printing process. As expected, the change in material didn't

take place immediately after receiving the control commands at locations 1-4. Instead, a delay was observed before the printed line changed its color.

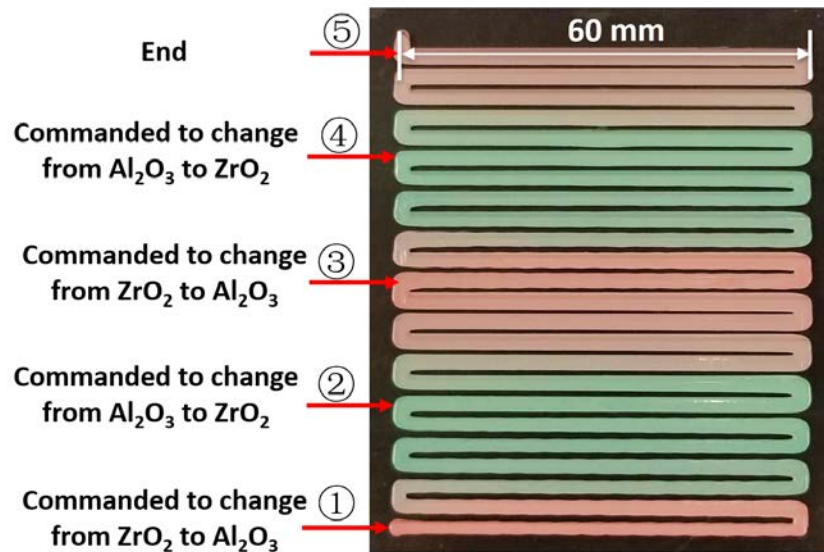


Figure 2. A single-bead serpentine printed using dynamic mixing device with graded materials (pink:  $\text{ZrO}_2$ , green:  $\text{Al}_2\text{O}_3$ ). The mixing blade was spinning at 900 rpm during the entire printing process.

### Determining the delay of changing material composition

The dried serpentine shaped specimen is shown in Figure 2 and Figure 3(a). The colors in Figure 3(a) indicated that the material composition changed periodically in four cycles as commanded. The pattern of material color change was similar in each cycle, indicating that the delay in composition transition was repeatable. Other than observing the material composition variation visually by color, EDS was also utilized on sintered specimens to obtain detailed measurements of composition at locations of interest. As shown in Figure 3(b), 42 locations of interest in cycle 1 were selected for EDS measurements. Locations 1 and 42 were the starting and ending locations of cycle 1, i.e., the locations where the tool head was commanded to switch from one material to another. The EDS measurements were taken at the surface of the specimen. At each location, the EDS measurement covered three areas of  $\sim 120 \mu\text{m}$  by  $120 \mu\text{m}$ . The percentages of Al atomic counts over the total atomic counts of Al, Zr, and Y of the three sampling areas for all locations are plotted in Figure 3(c). According to the graph in Figure 3(c), after the command to change material was received at location 1, the actual material composition started to change at location 7, and gradually transit to the desired material composition (100%  $\text{Al}_2\text{O}_3$ ). Location 38 was determined as the location where the transition of composition was completed. The stable material composition between locations 1 and 7 was characterized as the result of purging out the residual  $\text{ZrO}_2$  paste in the material outlet (shown in Figure 1(a)). The volume of paste being deposited between locations 1 and 7 was termed the delivery delay. On the other hand, the volume of paste being deposited between locations 7 and 38 was termed the transition delay, which was related to the paste streams propagating behavior in the flow path of the mixer, and the volume of the flow path. The delivery delay and the transition delay made up the total delay when changing material composition, and their volumes were quantified as 0.12 mL, 0.36 mL, and 0.48 mL,

respectively. As expected, the delivery delay (0.12 mL) was equal to the volume of the material outlet of the mixer. In the practice of printing laminar FGM samples, the total delay ( $V_{delay}$ ) was considered in the control scheme, and proper compensation was made to precisely deposit materials with desired compositions.

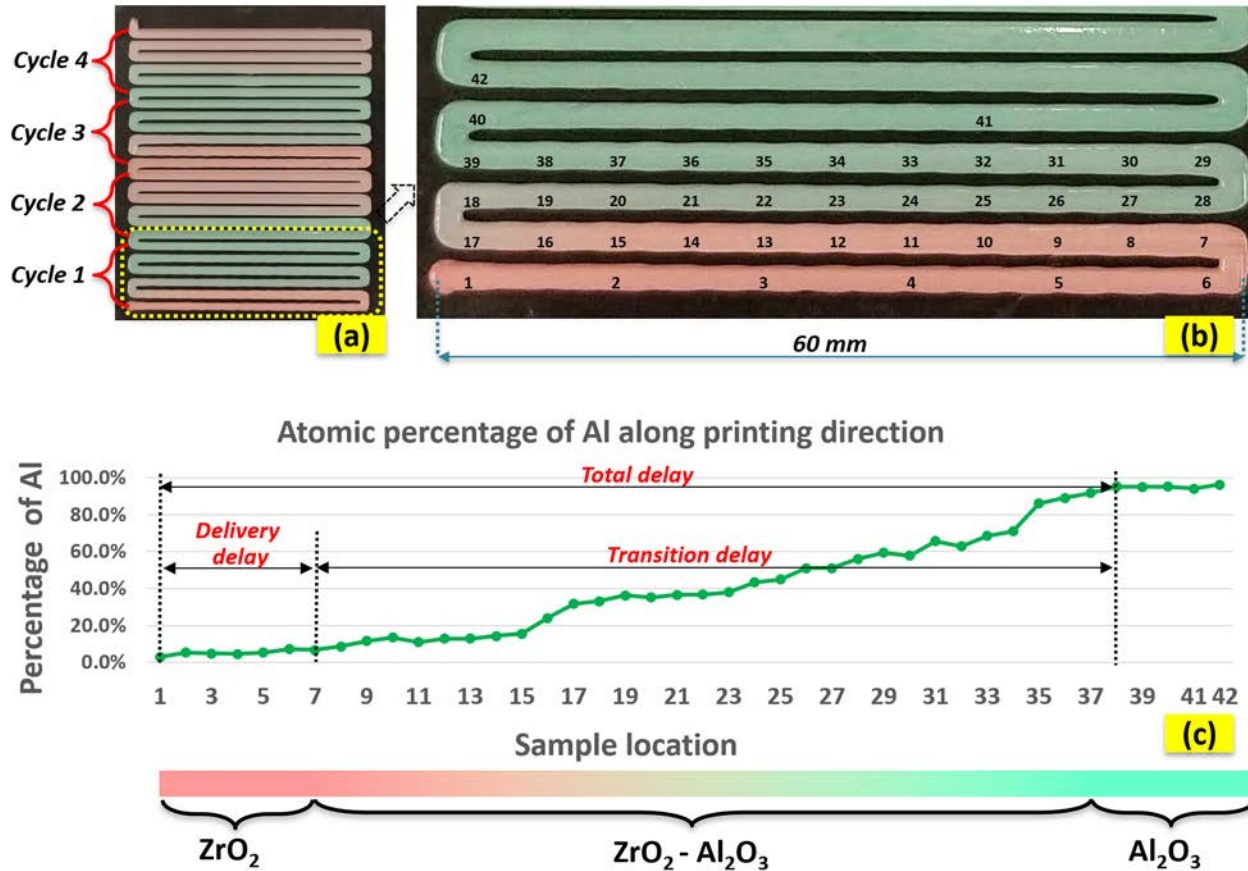


Figure 3. (a) Four cycles of the printed serpentine. (b) 42 sampling locations for EDS test on cycle 1 of the serpentine. (c) The atomic percentage of Al measured by EDS at different locations.

### Fabricating laminar $Al_2O_3/ ZrO_2$ FGM specimens

To examine the ability of the dynamic mixing tool head to accurately control the material composition, and to study the drying and sintering behavior of bulk FGM specimens, three groups of laminar FGM specimens graded from  $Al_2O_3$  to  $Al_2O_3/ZrO_2$  (50/50) were fabricated. Each group had three samples with different material gradients. The material gradient for the three types is shown in Figure 4. Type 1 had a 5 vol% increment of  $ZrO_2$  every one layer and hence grads from  $Al_2O_3$  to  $Al_2O_3/ZrO_2$  by 10 steps through 11 layers. Type 2 had a 10 vol% increment of  $ZrO_2$  every 2 layers hence grads from  $Al_2O_3$  to  $Al_2O_3/ZrO_2$  by 5 steps through 11 layers. Finally, Type 3 was transitioned from  $Al_2O_3$  directly to  $Al_2O_3/ZrO_2$  at the 6<sup>th</sup> layer of the 11-layer sample. All the FGM specimens were designed to have identical dimensions ( $70 \times 20 \times 6.6 \text{ mm}^3$ ) and numbers of layers to ensure a fair comparison of potential part deformation after sintering.

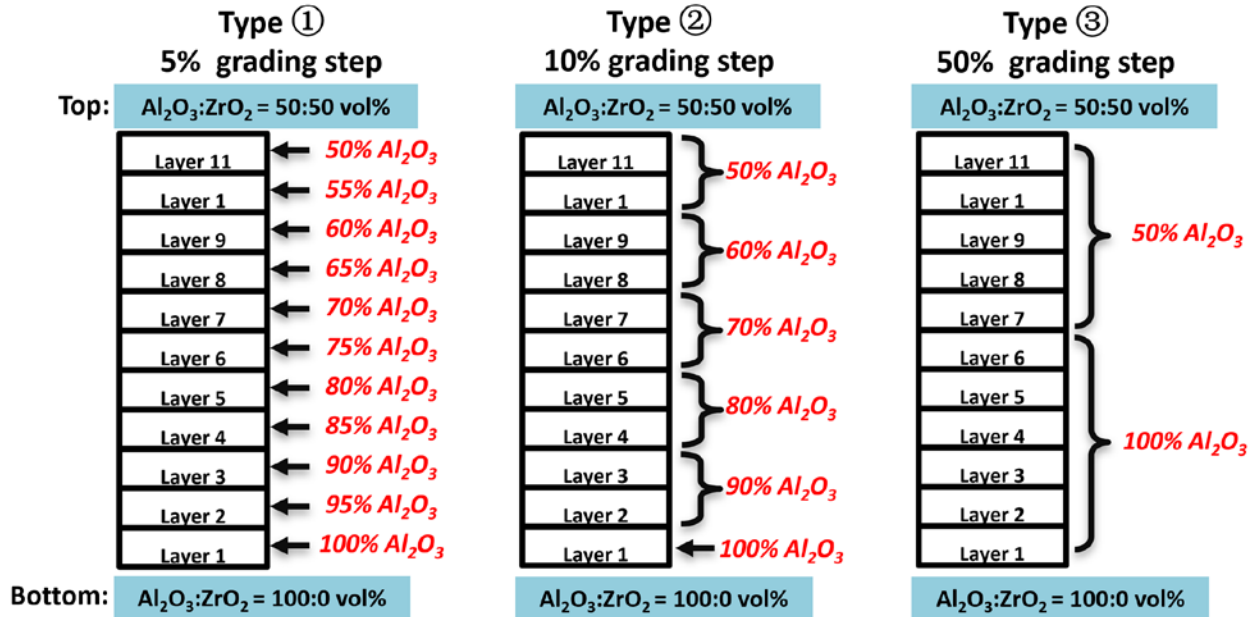


Figure 4. Design of material composition distribution in three types of FGM specimens.

Considering the significant delay ( $V_{delay} = 0.48 \text{ mL}$ ) of changing composition discussed in the previous section, each time a change of composition in a new layer was required, an additional purging process was conducted before the new layer was started. In the purging process, the dynamic mixing tool head was commanded to move out of the building substrate, extrude two pastes at predetermined flowrates for a certain volume  $V_{purge}$  until the materials at the nozzle tip reached the desired steady composition ( $V_{purge} \geq V_{delay}$ ), and was finally moved back to the building substrate to start the new layer. The entire printing and purging process was fully automated by G-Codes. A  $V_{purge}$  of 0.5 mL was used in this experiment. The printed FGM specimens were bulk dried in an environmental chamber for 12 hours where the temperature was controlled at 24°C and the relative humidity at 75%, then fired at 500°C for 1 hour to burn out the organic constituents including binder and dyes, and finally sintered at 1500°C for 1 hour to densify. The sintered specimens were characterized, and the result is presented in the following section. Figure 5 shows the printing process of an FGM specimen and dried FGM specimens of three types.

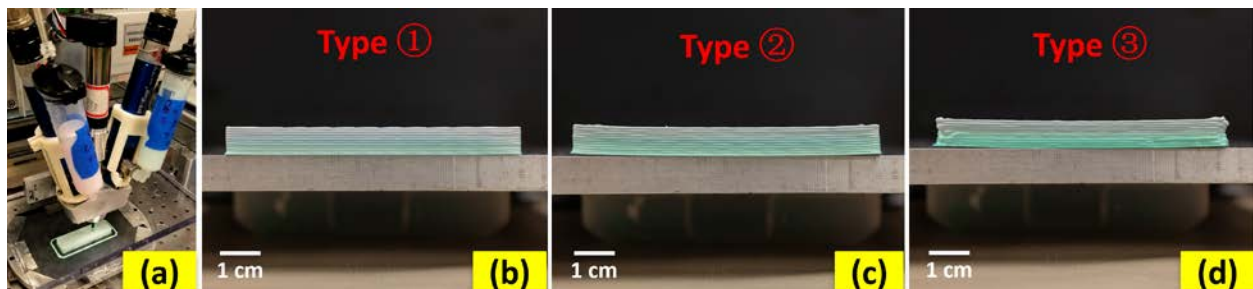


Figure 5. (a) A laminar  $\text{Al}_2\text{O}_3/\text{ZrO}_2$  FGM specimen being printed using the dynamic mixing tool head. (b) (c) (d) A group of laminar  $\text{Al}_2\text{O}_3/\text{ZrO}_2$  FGM specimens printed and dried.

## Results and Discussion

### Accuracy of material composition control

Two sintered FGM specimens from Type 1 were cut, and ground from the side for ~ 4 mm to reveal the inner cross-section as illustrated in Figure 6(b), then polished down to a 0.25-micron finish and coated with gold/palladium for EDS measurements. For all 11 layers in the two specimens, EDS intensity measurements were taken over 3 regions with approximately 120  $\mu\text{m}$  by 120  $\mu\text{m}$  areas. The ratio of Al peak vs. Zr peak, as well as the SEM images of two example layers, are shown in Figure 6(c)(d). The dark ( $\text{Al}_2\text{O}_3$ ) and bright ( $\text{ZrO}_2$ ) phases in the SEM images show a homogeneous distribution of the two materials.

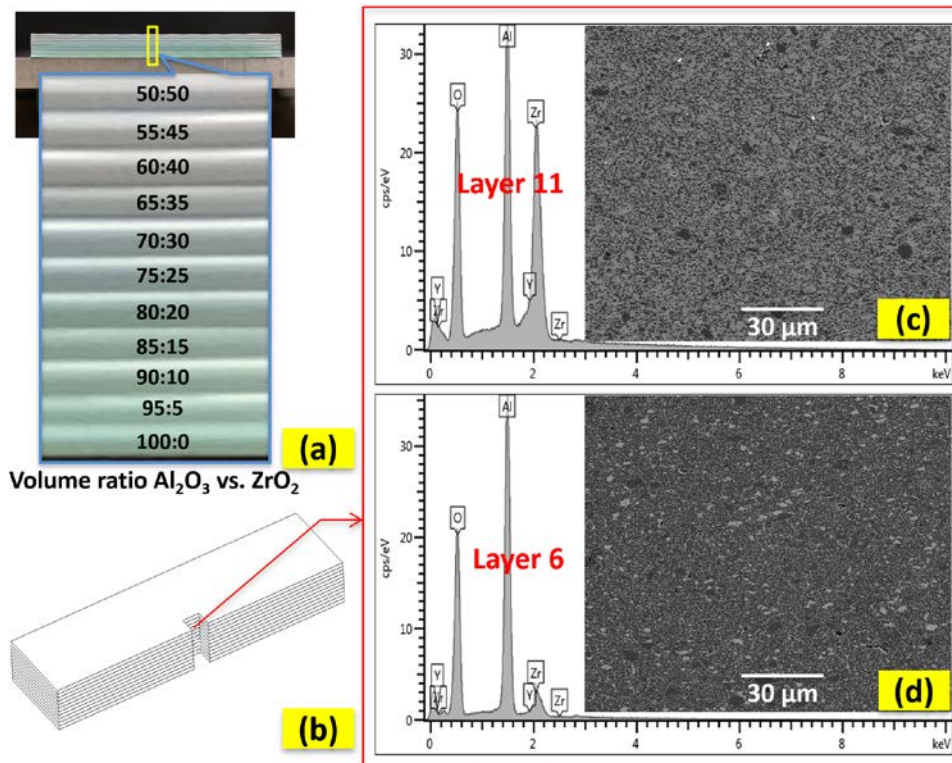


Figure 6. (a) A photo of a dried (not sintered) FGM specimen of Type 1, and a close-up view showing a color change of its layers. (b) Schematic showing the cross-section where EDS measurements were taken. (c) (d) EDS peaks and SEM images taken from layer 11 and 6 of the specimen.

The mean values of the measured atomic percentage of Al for layers 1-11 were plotted in Figure 7 by the solid line. Based on the designed volume ratio of the  $\text{Al}_2\text{O}_3$  and  $\text{ZrO}_2$  pastes, the solids loading of two pastes, density and molecular weight of the two materials, the nominal atomic percentages of Al in all layers were calculated and plotted in Figure 7 by the dashed line. The average error between the measured value and nominal value was 1% and the maximum discrepancy was 2%, indicating a good accuracy of the dynamic mixing tool head for controlling material composition.

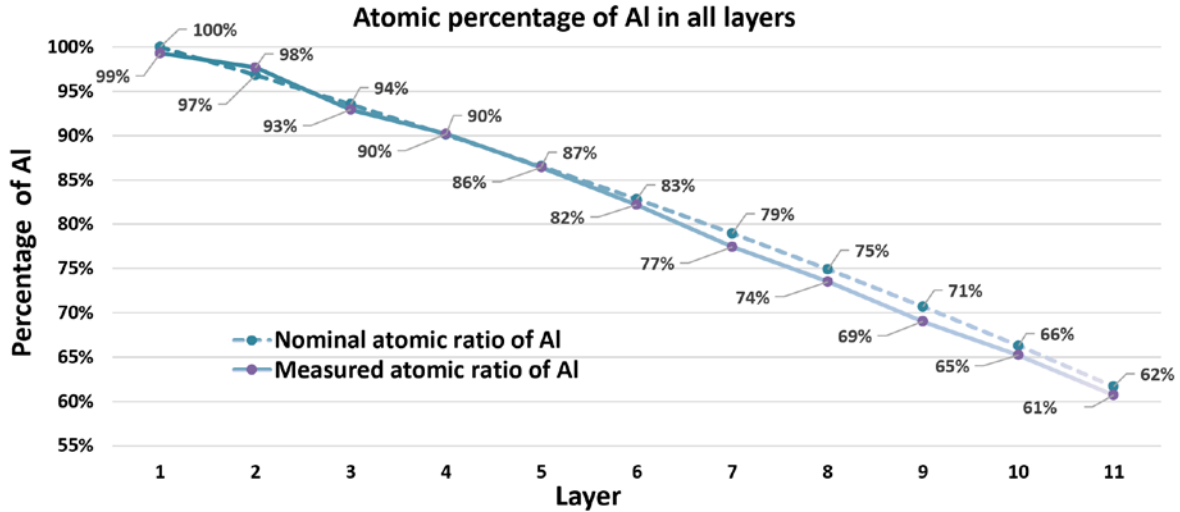


Figure 7. The atomic percentage of Al of each layer in the sintered FGM specimens.

### Deformation of specimens

After sintering, the 3 groups of colored  $\text{Al}_2\text{O}_3/\text{ZrO}_2$  specimens turned white since the organic dyes burned out during the firing process. Curling and delamination were observed in the sintered specimens. In order to quantify the deformation of each specimen, as shown in Figure 8, the specimens were flipped on a flat substrate to measure the heights at their center and two ends, from which the curling angles were calculated for every specimen. The quantified deformation of all FGM specimens is reported in Table 1.

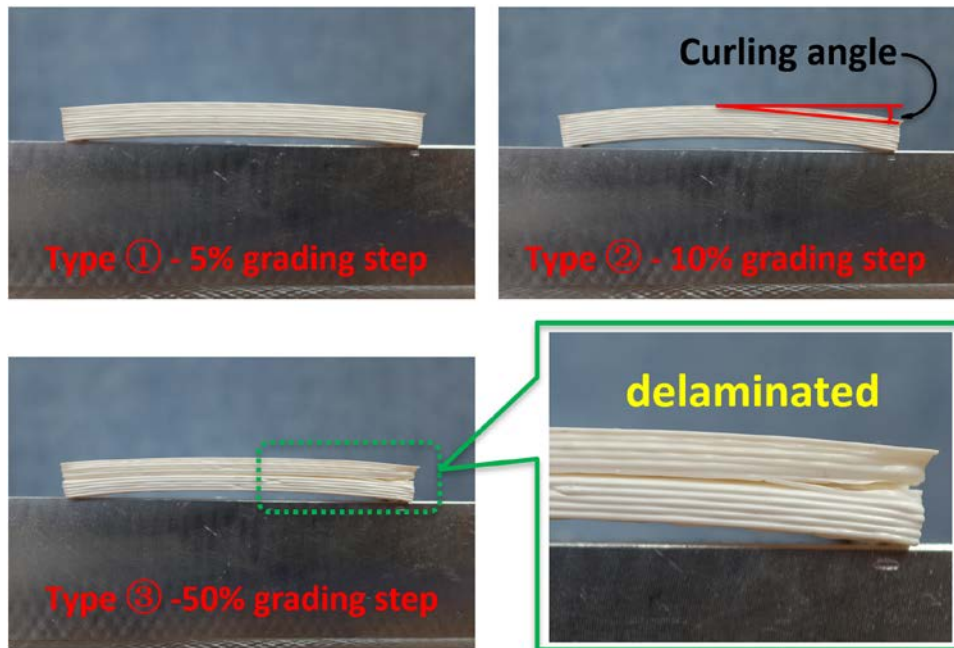


Figure 8. One group of FGM specimens after sintering, deformation, and failure were observed.

Table 1. Quantified deformation (curling angle) of each FGM specimen after sintering.

Grading Step	Curling Angle		
	Group 1	Group 2	Group 3
5% (Type 1)	2.7°	2.3°	2.9°
10% (Type 2)	3.6°	3.8°	3.7°
50% (Type 3)	4.9° (cracked)	delaminated	delaminated

### Vickers hardness

A sintered FGM specimen from Type 2 was cut, ground and polished in the similar way illustrated in Figure 6(b). Micro-indentation tests were performed at layers with different material compositions following ASTM C1327 standard [26]. For each layer with different compositions, 5 indentations were performed at different locations and the mean values of Vickers hardness were presented in Table 2, as well as their standard deviations.

Table 2. Vickers hardness of layers with different composition of Al<sub>2</sub>O<sub>3</sub>/ZrO<sub>2</sub> in an FGM specimen.

Layer	Volume ratio of Al <sub>2</sub> O <sub>3</sub> vs. ZrO <sub>2</sub>	Vickers Hardness (GPa)	
		Mean	Standard Deviation
10-11	50%:50%	15.0	0.31
8-9	60%:40%	16.0	0.23
6-7	70%:30%	16.3	0.14
4-5	80%:20%	16.9	0.41
2-3	90%:10%	17.5	0.28
1	100%:0%	18.4	0.32

### Discussion

Due to the delay of changing material composition using the dynamic mixing tool head, time and material waste are introduced to the printing of laminar FGM specimens when pastes are purged out before they reach a desired stable composition for a new layer. Moreover, the transition delay also limits the accuracy of controlling the in-plane gradient of composition in one layer. Minimizing the delay is always desirable for fabricating FGM components. The key point of minimizing the delay is to reduce the volume of the flow path. However, tighter flow path leads to an increase of back pressure, which requires higher extrusion pressure, especially for highly-viscous ceramic pastes. In addition, the fabrication of micro-sized mixing blades and flow paths is also challenging. A trade-off between the fast transition of composition and equipment investment is necessary, which will be investigated in the future, as well as the overall design of the dynamic mixer.

According to Figure 8 and Table 1, as the step of changing composition increased, the amount of deformation of the sintered FGM specimen increased until structural failure (cracking

and delamination) took place. Although less significant, a similar trend of deformation was also observed on the FGM specimens after they were bulk dried, as shown in Figure 5(b)(c)(d). The deformation occurred during the bulk drying process indicated a mismatch in drying shrinkage of the two pastes. Since the two pastes had the same (50 vol%) solids loading, the difference in shrinkage was believed to be caused by the different packing density of the particles in the two pastes after they were dried. On the other hand, the deformation occurred during the sintering process was believed to be caused by the mismatch of sintering shrinkage and thermal expansion of  $\text{Al}_2\text{O}_3$  and  $\text{ZrO}_2$ . Larger differences in material composition between layers lead to larger stresses caused by the mismatch of material properties, which explains the fact that the larger step of changing composition led to larger amounts of deformation. A smoother (reduced) gradient of material composition is likely to reduce the amount of deformation and the risk of part failure. Adjusting the inherent properties of the raw materials to reduce the mismatch of shrinkage could be another effective way of mitigating the stress and deformation. For example, according to the study of Sun *et.al.* [27], adjusting the particle size distribution of the  $\text{Al}_2\text{O}_3$  and  $\text{ZrO}_2$  powders could contribute to matching the shrinkage of layers with different  $\text{Al}_2\text{O}_3/\text{ZrO}_2$  ratios in the FGM specimens.

SEM images taken at the cross-section of the FGM specimens, of which two example images are shown in Figure 6, demonstrated a high homogeneity of the mixed  $\text{Al}_2\text{O}_3$  and  $\text{ZrO}_2$  phases. Vickers hardness reported in Table 2 demonstrated a clear trend of decreased hardness as the  $\text{ZrO}_2$  concentration was increased. The hardness values were in good agreement with data reported from other literature [27–29]. The hardness measurements at different locations for each composition were highly consistent according to their standard deviations, which is another evidence that the  $\text{Al}_2\text{O}_3$  and  $\text{ZrO}_2$  pastes were mixed to highly homogeneous.

## **Conclusions**

A dynamic extrusion-mixing device was developed for fabricating functionally graded materials (FGM) by the Ceramic On-Demand Extrusion process. The effectiveness of this device was validated by fabricating FGM specimens graded from pure  $\text{Al}_2\text{O}_3$  to  $\text{Al}_2\text{O}_3/\text{ZrO}_2$  with predetermined material gradients. The FGM specimens were sintered at 1500 °C and the material composition of each layer in the sintered FGM specimens was validated by measuring the atomic percentage of Al and Zr by energy dispersive spectroscopy (EDS), and compared to the original design of compositions. A 1% average error of material composition was observed from the comparison. Deformations were measured on the dried and sintered FGM specimens. Greater material composition gradients led to larger deformations of specimens. The Vickers hardness decreased from 18.4 GPa to 15.0 GPa as the volume percentage of  $\text{ZrO}_2$  increased from 0 to 50 vol% in  $\text{Al}_2\text{O}_3/\text{ZrO}_2$  layers.

## **Acknowledgments**

This work was funded by Honeywell Federal Manufacturing & Technologies under Contract No. DE-NA0002839 with the U.S. Department of Energy. The United States Government

retains and the publisher, by accepting the article for publication, acknowledges that the United States Government retains a non-exclusive, paid up, irrevocable, worldwide license to publish or reproduce the published form of this manuscript, or allow others to do so, for the United States Government purposes.

### References

- [1] S. Zhang, H. Miyanaji, L. Yang, A. Ali Zandinejad, J. Dilip, and B. Stucker, “An experimental study of ceramic dental porcelain materials using a 3D print (3DP) process,” *Proc. 25th Annu. Int. Solid Free. Fabr. Symp.*, pp. 991–1011, 2014.
- [2] H. Miyanaji, S. Zhang, A. Lassell, A. Zandinejad, and L. Yang, “Process development of porcelain ceramic material with binder jetting process for dental applications,” *J. Miner. Met. Mater. Soc.*, vol. 68, no. 3, pp. 831–841, 2016.
- [3] J. Cesarano, R. Segalman, and P. Calvert, “Robocasting provides moldless fabrication from slurry deposition,” *Ceram. Ind.*, vol. 148, no. 4, p. 94, 1998.
- [4] W. Li, A. Ghazanfari, D. McMillen, M. C. Leu, G. E. Hilmas, and J. Watts, “Fabricating ceramic components with water dissolvable support structures by the Ceramic On-Demand Extrusion process,” *CIRP Ann. - Manuf. Technol.*, vol. 66, no. 1, pp. 225–228, 2017.
- [5] M. Faes, J. Vleugels, F. Vogeler, and E. Ferraris, “Extrusion-based additive manufacturing of ZrO<sub>2</sub> using photoinitiated polymerization,” *CIRP J. Manuf. Sci. Technol.*, vol. 14, pp. 28–34, 2016.
- [6] K. K. B. Hon, L. Li, and I. M. Hutchings, “Direct writing technology—Advances and developments,” *CIRP Ann. - Manuf. Technol.*, vol. 57, no. 2, pp. 601–620, 2008.
- [7] A. Ghazanfari, W. Li, M. C. Leu, and G. E. Hilmas, “A novel freeform extrusion fabrication process for producing solid ceramic components with uniform layered radiation drying,” *Addit. Manuf.*, vol. 15, pp. 102–112, 2017.
- [8] J. Li, “An experimental study of fabrication temperature effect on aqueous extrusion freeform fabrication,” Missouri University of Science and Technology, 2015.
- [9] M. Schwentenwein and J. Homa, “Additive manufacturing of dense alumina ceramics,” *Int. J. Appl. Ceram. Technol.*, vol. 12, no. 1, pp. 1–7, 2015.
- [10] T. Chartier, C. Chaput, F. Doreau, and M. Loiseau, “Stereolithography of structural complex ceramic parts,” *J. Mater. Sci.*, vol. 37, no. 15, pp. 3141–3147, 2002.
- [11] P. Bertrand, F. Bayle, C. Combe, P. Goeuriot, and I. Smurov, “Ceramic components manufacturing by selective laser sintering,” *Appl. Surf. Sci.*, vol. 254, no. 4, pp. 989–992, 2007.

- [12] N. Kang *et al.*, “A novel approach to in-situ produce functionally graded silicon matrix composite materials by selective laser melting,” *Compos. Struct.*, vol. 172, pp. 251–258, 2017.
- [13] F. Niu, D. Wu, G. Ma, J. Wang, J. Zhuang, and Z. Jin, “Rapid fabrication of eutectic ceramic structures by laser engineered net shaping,” *Procedia CIRP*, vol. 42, pp. 91–95, 2016.
- [14] F. Niu, D. Wu, G. Ma, J. Wang, M. Guo, and B. Zhang, “Nanosized microstructure of Al<sub>2</sub>O<sub>3</sub>-ZrO<sub>2</sub> (Y<sub>2</sub>O<sub>3</sub>) eutectics fabricated by laser engineered net shaping,” *Scr. Mater.*, vol. 95, no. 1, pp. 39–41, 2015.
- [15] F. Niu, D. Wu, G. Ma, and B. Zhang, “Additive manufacturing of ceramic structures by laser engineered net shaping,” *Chinese J. Mech. Eng.*, vol. 28, no. 6, pp. 1117–1122, 2015.
- [16] A. Ghazanfari, W. Li, M. Leu, J. Watts, and G. Hilmas, “Mechanical characterization of parts produced by ceramic on-demand extrusion process,” *Int. J. Appl. Ceram. Technol.*, vol. 14, no. 3, pp. 486–494, 2017.
- [17] W. Li, A. Ghazanfari, D. McMillen, M. C. Leu, G. E. Hilmas, and J. Watts, “Characterization of zirconia specimens fabricated by ceramic on-demand extrusion,” *Ceram. Int.*, vol. 44, no. 11, pp. 12245–12252, 2018.
- [18] A. Ghazanfari, W. Li, M. C. Leu, J. L. Watts, and G. E. Hilmas, “Additive manufacturing and mechanical characterization of high density fully stabilized zirconia,” *Ceram. Int.*, vol. 43, no. 8, pp. 6082–6088, 2017.
- [19] L. Yan, X. Chen, Y. Zhang, J. W. Newkirk, and F. Liou, “Fabrication of functionally graded Ti and  $\gamma$ -TiAl by laser metal deposition,” *JOM*, vol. 69, no. 12, pp. 2756–2761, 2017.
- [20] L. Yang, H. Miyajima, D. Janaki Ram, A. Zandinejad, and S. Zhang, “Functionally graded ceramic based materials using additive manufacturing: review and progress,” *Addit. Manuf. Strateg. Technol. Adv. Ceram.*, vol. 258, pp. 43–55, 2016.
- [21] W. Li, L. Yan, X. Chen, J. Zhang, X. Zhang, and F. Liou, “Directed energy depositing a new Fe-Cr-Ni alloy with gradually changing composition with elemental powder mixes and particle size’ effect in fabrication process,” *J. Mater. Process. Technol.*, vol. 255, pp. 96–104, 2018.
- [22] Y. Li, Y. Shen, C.-H. Hung, M. C. Leu, and H.-L. Tsai, “Additive manufacturing of Zr-based metallic glass structures on 304 stainless steel substrates via V/Ti/Zr intermediate layers,” *Mater. Sci. Eng. A*, vol. 729, pp. 185–195, 2018.
- [23] M. N. Rahaman, A. Yao, B. S. Bal, J. P. Garino, and M. D. Ries, “Ceramics for prosthetic hip and knee joint replacement,” *J. Am. Ceram. Soc.*, vol. 90, no. 7, pp. 1965–1988, 2007.
- [24] P. Muller, P. Mognol, and J.-Y. Hascoe, “Functionally graded material (FGM)parts: from design to the manufacturing simulation,” *Proc. ASME 2012 11th Bienn. Conf. Eng. Syst. Des. Anal.*, pp. 1–9, 2018.

- [25] W. Li, A. Ghazanfari, M. C. Leu, and R. G. Landers, "Extrusion-on-demand methods for high solids loading ceramic paste in freeform extrusion fabrication," *Virtual Phys. Prototyp.*, vol. 12, no. 3, pp. 193–205, 2017.
- [26] ASTM C1327, "Standard test method for Vickers indentation hardness of advanced ceramics," West Conshohocken, PA, 2015.
- [27] L. Sun, A. Sneller, and P. Kwon, "Fabrication of alumina/zirconia functionally graded material: From optimization of processing parameters to phenomenological constitutive models," *Mater. Sci. Eng. A*, vol. 488, no. 1–2, pp. 31–38, 2008.
- [28] C. Kaya, "Al<sub>2</sub>O<sub>3</sub>-Y-TZP/Al<sub>2</sub>O<sub>3</sub> functionally graded composites of tubular shape from nano-sols using double-step electrophoretic deposition," *J. Eur. Ceram. Soc.*, vol. 23, no. 10, pp. 1655–1660, 2003.
- [29] A. Nevarez-Rascon, A. Aguilar-Elguezabal, E. Orrantia, and M. H. Bocanegra-Bernal, "On the wide range of mechanical properties of ZTA and ATZ based dental ceramic composites by varying the Al<sub>2</sub>O<sub>3</sub> and ZrO<sub>2</sub> content," *Int. J. Refract. Met. Hard Mater.*, vol. 27, no. 6, pp. 962–970, 2009.
- [30] Z. Wu, W. Liu, H. Wu, R. Huang, R. He, Q. Jiang, Y. Chen, X. Ji, Z. Tian, and S. Wu, "Research into the mechanical properties, sintering mechanism and microstructure evolution of Al<sub>2</sub>O<sub>3</sub>-ZrO<sub>2</sub> composites fabricated by a stereolithography-based 3D printing method," *Mater. Chem. Phys.*, vol. 207, pp. 1–10, 2018.